Break-up effect on the elastic scattering and the optical potential of ^{11}Li

K. Yabana,[1,2,*] Y. Ogawa,[3] and Y. Suzuki[1]
[1]*Department of Physics, Niigata University, Ikarashi-2, Niigata 950-21, Japan*
[2]*National Superconducting Cyclotron Laboratory, Michigan State University, East Lansing, Michigan 48824*
[3]*Graduate School of Science and Technology, Niigata University, Ikarashi-2, Niigata 950-21, Japan*
(Received 21 January 1992)

The elastic scattering of weakly bound projectiles such as deuteron and ^{11}Li nucleus are examined including the break-up process to the continuum excited states. The eikonal approximation is employed to derive the optical potential which includes the dynamical polarization potential due to the break-up process. The dynamical polarization potential is realized to be closely related to the fluctuation of the constituents of the projectile nucleus in its ground state. Strong effect of the break-up process on the ^{11}Li-^{12}C optical potential is found, which is qualitatively similar to those known for the deuteron optical potential. The elastic scattering differential cross section for ^{11}Li-^{12}C is calculated with the obtained optical potential. It is found that the scattering cross section decreases rapidly for large scattering angle compared with the ^{9}Li elastic scattering.

PACS number(s): 24.10.Ht, 25.70.Bc, 25.45.De

I. INTRODUCTION

The halo structure of the neutron drip-line nuclei has been extensively studied with the secondary radioactive beam. The ^{11}Li nucleus has attracted much experimental and theoretical interest as a typical case. Since the successful measurement of the interaction cross section has shown the anomalously large matter distribution of ^{11}Li nucleus [1], the studies of the halo structure of the neutron drip-line nuclei have been achieved and are under progress making use of various kinds of reaction mechanisms. Among them is the elastic scattering which we are going to discuss in this paper. The theoretical study of this subject has already been undertaken by both the phenomenological [2] and microscopic approaches [3,4].

The ground state of ^{11}Li nucleus is just below the ^{9}Li$+n+n$ three-body threshold. There exists no bound state for the subsystems, ^{9}Li$+n$ and $n+n$. It is expected that the ground-state structure of ^{11}Li nucleus is well described by the (^{9}Li$+n+n$) three-body model, where ^{9}Li nucleus is in the ground state and the halo is composed of the two neutrons which are bound weakly to the ^{9}Li nucleus. (We will call these two neutrons as "halo neutron.") Such a three-body picture is strongly supported by the microscopic three-body calculations [5,6].

For the heavy ion elastic scattering including weakly bound nuclei, it has been known that the double folding model for the real part of the optical potential fails [7]. The studies including the break-up process have revealed the important role of the break-up process in the elastic scattering and the optical potential, particularly in the cases of deuteron projectile [8,9] and the light heavy ion projectile [10]. It is strongly expected that the break-up of the ^{11}Li nucleus into ^{9}Li$+n+n$ three-body continuum states contributes significantly to the elastic scattering process.

In our previous paper [11] which we will abbreviate as I in the following, we have proposed to describe the reaction of the drip-line nucleus in the intermediate energy region by the use of the eikonal approximation in a direct reaction framework. We have found there the large cross section of $^{11}\text{Li}\rightarrow(^{9}\text{Li}+n+n)$ three-body break-up reaction. We will extend the framework of I so as to analyze the optical potential and the elastic scattering of ^{11}Li.

Recently Canto *et al.* [3] have discussed, in an approach intimately related to us, the effect of the break-up process on the optical potential and the elastic scattering of ^{11}Li. They mainly discussed the imaginary part of the dynamical polarization potential due to the break-up process. In this paper we will show that the break-up process appreciably affects the real part of the optical potential as well as the imaginary part. Our approach is also advantageous in that the relation between the dynamical polarization potential and the halo wave function is quite transparent.

The construction of the paper is the following. In Sec. II, the optical potential and the elastic scattering for the case of the deuteron projectile are examined, for the purpose of showing the usefulness of our framework in investigating the effect of the break-up process on the optical potential and elastic scattering. In Sec. III, the optical potential for ^{11}Li-^{12}C system is discussed. In Sec. IV, the elastic scattering of ^{11}Li-^{12}C system is discussed. In Sec. V, concluding remarks are presented.

II. DEUTERON PROJECTILE CASE

The important role of the break-up process of the deuteron into $(p+n)$ continuum states on the elastic scattering process has been studied under the adiabatic approximation [8] and the coupled discretized continuum

*Present address.

channels approaches (CDCC) [9,12]. We consider the same problem, further simplifying by employing the eikonal and the adiabatic approximations. Assuming the straight line trajectory of the deuteron, we no longer need to solve any quantum mechanical equation. Furthermore it provides us with the understanding of the break-up effect in terms of the proton-neutron relative motion in the deuteron ground state.

A. Elastic scattering amplitude

We describe the deuteron reaction in terms of the $(p+n)$-target nucleus three-body model. The Schrödinger equation,

$$\left[\frac{P^2}{2\mu}+h_0+U_p(\mathbf{r}_p)+U_n(\mathbf{r}_n)\right]\Psi(\mathbf{r}_p,\mathbf{r}_n)=E\Psi(\mathbf{r}_p,\mathbf{r}_n), \quad (2.1)$$

describes the deuteron reaction with target nucleus where the target nucleus remains in the ground state throughout the reaction. In Eq. (2.1), $\mathbf{P}$ represents the center-of-mass momentum of the deuteron, μ is the reduced mass of the deuteron and the target nucleus. h_0 is the internal Hamiltonian of the deuteron. $U_p(\mathbf{r})$ and $U_n(\mathbf{r})$ are the proton- and neutron-target nucleus optical potentials, respectively. $\mathbf{r}_p$ and $\mathbf{r}_n$ are the coordinates of the proton and the neutron with respect to the target nucleus. The spin degree of freedom is ignored for simplicity.

We employ the eikonal and the adiabatic approximations to solve Eq. (2.1), as we did in I. The eikonal approximation assumes that the deuteron moves along the straight line trajectory specified by the impact parameter $\mathbf{b}$. The adiabatic approximation assumes that the internal motion of the proton and the neutron is at rest during the collision, and amounts to neglecting h_0 in solving Eq. (2.1). Under these approximations, the elastic scattering amplitude is given by

$$f_{\rm el}(\mathbf{q})=-\frac{iK}{2\pi}\int d\mathbf{b}\, e^{-i\mathbf{q}\cdot\mathbf{b}}\{\langle\phi_0|\exp[i\chi_p(\mathbf{b}+\mathbf{s}/2)+i\chi_n(\mathbf{b}-\mathbf{s}/2)]|\phi_0\rangle-1\}\ . \quad (2.2)$$

ϕ_0 represents the ground-state wave function of the deuteron. $\mathbf{s}$ is the projection of the vector $\mathbf{r}=\mathbf{r}_p-\mathbf{r}_n$ onto the x-y plane where we assume the incident direction to be parallel to the z axis. χ_p and χ_n are the phase shift functions and are defined by

$$\chi_{p,n}(\mathbf{b})=-\frac{1}{\hbar v}\int_{-\infty}^{+\infty}dz\, U_{p,n}(\mathbf{b}+z\mathbf{e}_z)\ . \quad (2.3)$$

B. Optical potential

According to the prescription proposed by Glauber [13], we can construct the local, energy-dependent, optical potential $U_{\rm opt}(R)$ in the following way. Define the optical phase shift function $\chi_{\rm opt}(b)$ by

$$e^{i\chi_{\rm opt}(b)}=\langle\phi_0|\exp[i\chi_p(\mathbf{b}+\mathbf{s}/2)+i\chi_n(\mathbf{b}-\mathbf{s}/2)]|\phi_0\rangle\ . \quad (2.4)$$

Then we construct the potential which gives the same phase shift function as $\chi_{\rm opt}(b)$. Assuming that the optical potential is local and spherically symmetric, it is uniquely obtained as $[U_{\rm opt}(\infty)=0]$

$$U_{\rm opt}(R)=\frac{\hbar v}{\pi}\frac{1}{R}\frac{d}{dR}\int_R^{+\infty}b\,db\,\frac{\chi_{\rm opt}(b)}{\sqrt{b^2-R^2}}$$

$$=\frac{\hbar v}{\pi}\int_0^{+\infty}dx\,\frac{\chi'_{\rm opt}(\sqrt{R^2+x^2})}{\sqrt{R^2+x^2}}\ . \quad (2.5)$$

To discuss the relation to the single folding model, let us introduce the cumulant expansion [13] for the optical phase shift function $\chi_{\rm opt}(b)$. Denoting $\chi_p(\mathbf{b}+\mathbf{s}/2)+\chi_n(\mathbf{b}-\mathbf{s}/2)$ by $\chi_{pn}(\mathbf{b},\mathbf{s})$, we get

$$\chi_{\rm opt}(b)=\sum_{k=1}^{+\infty}\chi^{(k)}(b)\ . \quad (2.6)$$

The first few terms of the expansion are given by

$$i\chi^{(1)}(b)=\langle i\chi_{pn}\rangle\ ,$$
$$i\chi^{(2)}(b)=\frac{1}{2!}\langle(i\chi_{pn}-\langle i\chi_{pn}\rangle)^2\rangle\ , \quad (2.7)$$
$$i\chi^{(3)}(b)=\frac{1}{3!}\langle(i\chi_{pn}-\langle i\chi_{pn}\rangle)^3\rangle\ ,$$

where the notation $\langle\cdots\rangle$ represents the matrix element with respect to the wave function ϕ_0, for example,

$$\langle i\chi_{pn}\rangle=\langle\phi_0|i\chi_{pn}(\mathbf{b},\mathbf{s})|\phi_0\rangle\ . \quad (2.8)$$

For each term of the cumulant expansion of Eq. (2.7), we have the corresponding decomposition of the optical potential

$$U_{\rm opt}(R)=\sum_{k=1}^{+\infty}U^{(k)}(R)\ . \quad (2.9)$$

As is verified easily, the first-order term just coincides with the optical potential obtained by the single folding model,

$$U^{(1)}(R)=\int d\mathbf{r}|\phi_0(\mathbf{r})|^2[U_p(\mathbf{R}+\mathbf{r}/2)+U_n(\mathbf{R}-\mathbf{r}/2)]\ . \quad (2.10)$$

The remainder of the expansion of Eq. (2.9) thus gives the dynamical polarization potential

$$\Delta U(R)=U_{\rm opt}(R)-U^{(1)}(R)=\sum_{k=2}^{+\infty}U^{(k)}(R)\ . \quad (2.11)$$

The cumulant expansion is an expansion with respect to the fluctuation of the internal proton-neutron motion in the ground state of the deuteron. Neglection of the fluctuation gives us the single folding model. The dynamical polarization potential defined by Eq. (2.11) thus reflects the extent of the fluctuation. It is evident that the dynamical polarization potential becomes significant for the projectile whose ground state is weakly bound and possesses large fluctuation.

C. Analysis of d-^{58}Ni reaction

We analyze the optical potential of the deuteron with ^{58}Ni at $E_d = 80$ MeV. We analyzed various cross sections for this system in I. As in I, the internal wave function of the deuteron is taken to be S state. The optical potentials of p-^{58}Ni and n-^{58}Ni are chosen to be the conventional Woods-Saxon shape. No spin-orbit force is included. Parameters of the potentials are the same as those employed in Ref. [12] for the analysis of CDCC method. We neglect the effect of the Coulomb break-up process, that is, we assume that the Coulomb force between the deuteron and the target nucleus works between the center of masses of both nuclei.

In Fig. 1, solid curves show the deuteron optical potential given by Eq. (2.5). The optical potential by the single folding model, $U^{(1)}(R)$, is also shown by dashed curves. The dynamical polarization potential is shown in Fig. 2 by the solid curve which is the difference between the solid and dashed curves in Fig. 1. The repulsive break-up effect on the real part of the optical potential, which has been stressed as the common feature of the weakly bound projectiles [9,10], is clearly seen in the surface region. The imaginary part increases, which is thought to come from the loss of the flux due to the elastic break-up process.

Also shown in Fig. 2 are the first few terms of the cumulant expansion of the dynamical polarization potential defined in Eq. (2.9). Inclusion of up to fourth-order contribution is presented. It should be noted that the second-order contribution, $U^{(2)}(R)$, is qualitatively similar to the full dynamical polarization potential, though the higher-order contributions even higher than fourth order are required for the quantitative discussion.

It will be worthwhile to further investigate the second-order potential, $U^{(2)}(R)$, since it gives the correct sign of the dynamical polarization potential and its structure is fairly simple. By its definition, the second-order potential reflects the fluctuation of the phase shift function with respect to the internal motion of the deuteron. Decompose the phase shift function, $\chi_{pn}(\mathbf{b},\mathbf{s})$, into the real and the imaginary parts, $\chi_{pn} = \mathrm{Re}\chi_{pn} + i\,\mathrm{Im}\chi_{pn}$, each term of which comes from the real and imaginary parts of the nucleon-target nucleus optical potential, respectively. We note that both $\mathrm{Re}\chi_{pn}$ and $\mathrm{Im}\chi_{pn}$ are positive definite since both the real and imaginary parts of the nucleon-nucleus optical potential are negative for whole spatial region [see Eq. (2.3)]. The second-order optical phase shift function defined by Eq. (2.7) can be expressed as

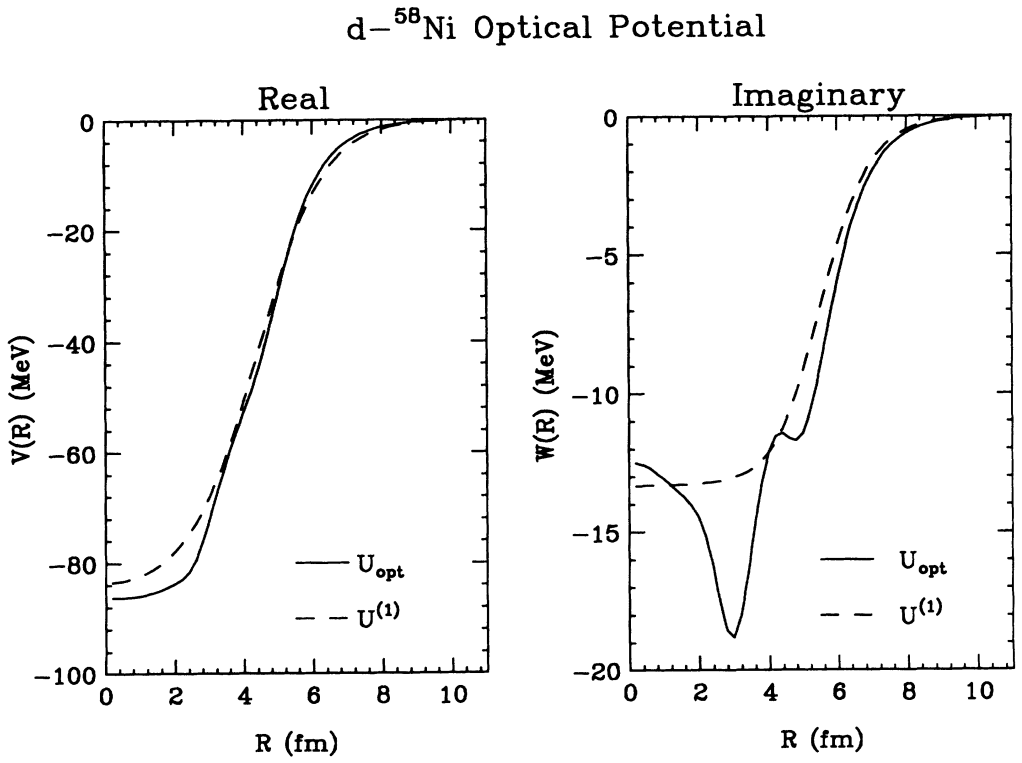

FIG. 1. The optical potential for the d-^{58}Ni system at $E = 80$ MeV. Solid curves include the break-up effect while dashed curves are the single folding model.

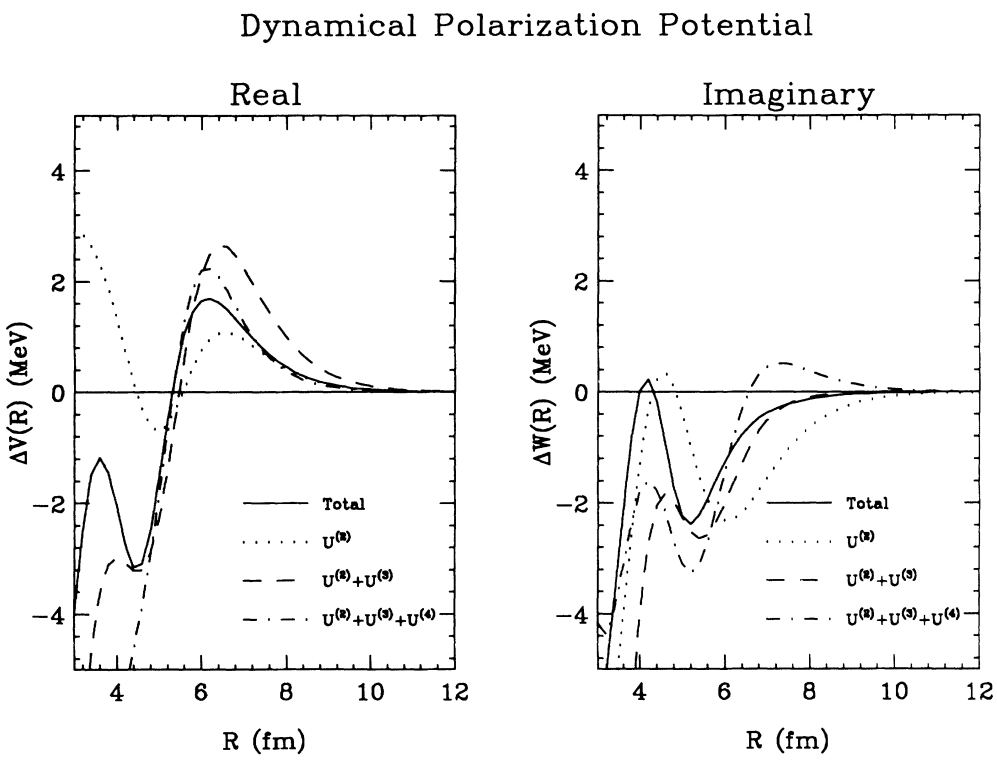

FIG. 2. The dynamical polarization potential of the d-^{58}Ni system (solid curves) and its decomposition into the cumulant expansion. The contributions up to the second, third, and fourth order are shown by dotted, dashed, and dot-dashed curves, respectively.

$$\begin{aligned} \mathrm{Re}\chi^{(2)}(b) &= \langle \mathrm{Re}\chi_{pn} \rangle \langle \mathrm{Im}\chi_{pn} \rangle - \langle \mathrm{Re}\chi_{pn} \mathrm{Im}\chi_{pn} \rangle = -\langle (\mathrm{Re}\chi_{pn} - \langle \mathrm{Re}\chi_{pn} \rangle)(\mathrm{Im}\chi_{pn} - \langle \mathrm{Im}\chi_{pn} \rangle) \rangle \ , \\ \mathrm{Im}\chi^{(2)}(b) &= \tfrac{1}{2}[\{\langle (\mathrm{Re}\chi_{pn})^2 \rangle - \langle \mathrm{Re}\chi_{pn} \rangle^2\} - \{\langle (\mathrm{Im}\chi_{pn})^2 \rangle - \langle \mathrm{Im}\chi_{pn} \rangle^2\}] \ . \end{aligned} \tag{2.12}$$

For not very high incident energy, both the real and imaginary parts of the phase shift function are expected to be of the same sign and nearly proportional, $\mathrm{Re}\chi_{pn} \propto \mathrm{Im}\chi_{pn}$, because of the near proportionality of $\mathrm{Re}U_{p,n}$ and $\mathrm{Im}U_{p,n}$. Then we find that $\mathrm{Re}\chi^{(2)}$ becomes negative. The second-order potential has opposite sign to $\chi^{(2)}$ [see Eq. (2.3)] and will be positive.

As for the imaginary part, it is a difference between the fluctuations of the real and the imaginary parts of the phase shift function. Since the shapes of the real and the imaginary parts of the phase shift function are similar, its sign depends on the strength of the optical potential. For the energy region below 100 MeV/nucleon, the real part of the optical potential is dominant. We then get a positive contribution for $\chi^{(2)}(b)$ and negative contribution for $\mathrm{Im}U^{(2)}$. The above discussion explains the sign of the second-order potential shown in Fig. 2.

In Fig. 3, we show the angular distribution of the deuteron scattering. Dots are the experimental result [14]. The dotted curve is the analysis by the CDCC method which solves Eq. (2.1) quantum mechanically. The solid curve represents the cross section calculated with the optical potential defined by Eq. (2.5), that is, we solved the Schrödinger equation with the optical poten-

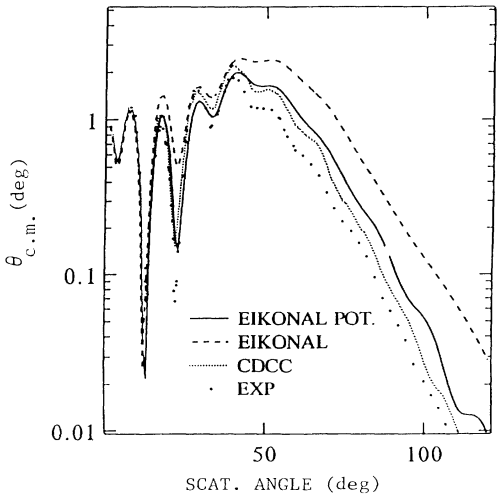

FIG. 3. Angular distribution of d-^{58}Ni elastic scattering at $E=80$ MeV, quoted from I. The dashed curve is calculated by the eikonal approximation, the dotted curve by the coupled discretized continuum channels method [9], and the solid curve is calculated with the optical potential which is constructed by the use of the eikonal approximation. Dots are the experimental data [14].

tial of Eq. (2.5) quantum mechanically. Nice reproduction of the CDCC result indicates that the reaction mechanisms including break-up process are properly taken into account in the optical potential of Eq. (2.5). The dashed curve is the cross section by the scattering amplitude of Eq. (2.2), namely, the cross section by the optical potential of Eq. (2.5) under the eikonal approximation. The momentum transfer q is related to the center-of-mass scattering angle θ by $q=2K\sin(\theta/2)$. The difference between the solid and dashed curves represents the accuracy of the eikonal approximation in calculating the elastic differential cross section. Though we used the eikonal and adiabatic approximations in deriving the optical potential of Eq. (2.5), the error due to the straight line trajectory for calculating the angular distribution of the elastic scattering is considerably removed by solving quantum mechanically the Schrödinger equation with the optical potential of Eq. (2.5).

III. OPTICAL POTENTIAL OF ^{11}Li

We assume that the ground-state structure of ^{11}Li is well described by the (^{9}Li$+n+n$) three-body model. We describe the ^{11}Li reaction by the (^{9}Li$+n+n$)-target nucleus four-body model:

$$\left[\frac{P^2}{2\mu}+h_0+U(\mathbf{R},\mathbf{r}_1,\mathbf{r}_2)\right]\Psi(\mathbf{R},\mathbf{r}_1,\mathbf{r}_2)=E\Psi(\mathbf{R},\mathbf{r}_1,\mathbf{r}_2)\ , \tag{3.1}$$

$$U(\mathbf{R},\mathbf{r}_1,\mathbf{r}_2)=U_{^9\mathrm{Li}}(R)+U_n(\mathbf{R}+\mathbf{r}_1)+U_n(\mathbf{R}+\mathbf{r}_2)\ . \tag{3.2}$$

$\mathbf{R},\mathbf{P}$ represent the relative coordinate and the momentum between ^{11}Li and the target nucleus, respectively. $\mathbf{r}_i$ is the coordinate vector of ith neutron with respect to ^{9}Li. μ is the reduced mass of ^{11}Li and target nucleus. h_0 is the internal Hamiltonian of ^{11}Li as a three-body system. $U_{^9\mathrm{Li}}(R)$ and $U_n(r)$ are the optical potentials of ^{9}Li- and neutron-target nucleus, respectively. For simplicity, we ignore the difference between the center of masses of ^{11}Li and ^{9}Li.

The wave function $\Psi(\mathbf{R},\mathbf{r}_1,\mathbf{r}_2)$ describes the reaction process where both ^{9}Li and target nuclei are in their ground states. We presented in I detailed discussion of the reaction dynamics involved in Eq. (3.1) under the eikonal and the adiabatic approximations. Under the approximations, the elastic scattering amplitude is given by

$$f_{\mathrm{el}}(\mathbf{q})=-\frac{iK}{2\pi}\int d\mathbf{b}\,e^{-i\mathbf{q}\cdot\mathbf{b}}\{\langle\phi_0|e^{-i\chi(\mathbf{b},\mathbf{s}_1,\mathbf{s}_2)}|\phi_0\rangle-1\}\ , \tag{3.3}$$

$$\chi(\mathbf{b},\mathbf{s}_1,\mathbf{s}_2)=\chi_{^9\mathrm{Li}}(b)+\chi_n(\mathbf{b}+\mathbf{s}_1)+\chi_n(\mathbf{b}+\mathbf{s}_2), \tag{3.4}$$

where K is the relative wave number. $\mathbf{s}_i$ is the projection of $\mathbf{r}_i$ onto the plane perpendicular to the incident direction. ϕ_0 represents the ground-state internal wave function of ^{11}Li as a three-body system and satisfies

$$h_0\phi_0=\epsilon_0\phi_0\ . \tag{3.5}$$

$\chi_{^9\mathrm{Li}}(b)$ and $\chi_n(b)$ are the phase shift functions for $U_{^9\mathrm{Li}}(R)$ and $U_n(r)$, respectively.

Let us define the optical phase shift function $\chi_{\mathrm{opt}}(b)$ by

$$e^{i\chi_{\mathrm{opt}}(b)}=\langle\phi_0|e^{i\chi(\mathbf{b},\mathbf{s}_1,\mathbf{s}_2)}|\phi_0\rangle=e^{i\chi_{^9\mathrm{Li}}(b)+i\chi_{2n}(b)}\ , \tag{3.6}$$

$$e^{i\chi_{2n}(b)}=\langle\phi_0|e^{i\chi_n(\mathbf{b}+\mathbf{s}_1)+i\chi_n(\mathbf{b}+\mathbf{s}_2)}|\phi_0\rangle\ . \tag{3.7}$$

The optical potential is obtained from $\chi_{\mathrm{opt}}(b)$ by the same formula as Eq. (2.5). As $\chi_{\mathrm{opt}}(b)$ is given as the sum of $\chi_{^9\mathrm{Li}}(b)$ and $\chi_{2n}(b)$, the optical potential is also given as the sum of ^{9}Li and the halo-neutron contributions,

$$U_{\mathrm{opt}}(R)=U_{^9\mathrm{Li}}(R)+U_{2n}(R)\ , \tag{3.8}$$

$U_{^9\mathrm{Li}}(R)$ is the same potential of ^{9}Li-target nucleus as we employed in Eq. (3.1) as input. $U_{2n}(R)$ is obtainable from $\chi_{2n}(b)$ by the same procedure as Eq. (2.5) and includes the effect of the halo-neutron break-up.

As we have done in the deuteron case, we introduce the cumulant expansion for the phase shift function and the optical potential to the halo-neutron part,

$$i\chi_{2n}(b)=\sum_{k=1}^{+\infty} i\chi_{2n}^{(k)}(b)\ , \tag{3.9}$$

$$U_{2n}(R)=\sum_{k=1}^{+\infty} U_{2n}^{(k)}(R)\ . \tag{3.10}$$

Each term of the expanded phase shift function is defined in the same way as Eq. (2.7).

The lowest-order term gives the single folding model,

$$U_{2n}^{(1)}(R)=\int d\mathbf{r}\,\rho_{2n}(r)U_n(\mathbf{R}-\mathbf{r})\ , \tag{3.11}$$

where $\rho_{2n}(r)$ represents the density distribution of the halo neutron. The single folding potential of ^{11}Li-target nucleus is given by

$$U_{\mathrm{fold}}(R)=U_{^9\mathrm{Li}}(R)+U_{2n}^{(1)}(R)\ . \tag{3.12}$$

The remainder of the expansion of Eq. (3.10) gives the dynamical polarization potential which reflects the break-up process of ^{11}Li into (^{9}Li$+n+n$) three-body continuum states,

$$\Delta U(R)=U_{2n}(R)-U_{2n}^{(1)}(R)=\sum_{k=2}^{+\infty} U_{2n}^{(k)}(R)\ . \tag{3.13}$$

As an example, we will analyze the optical potential of the ^{11}Li-^{12}C system. First we discuss the radial dependence of the potential at $E/A=60$ MeV. We utilize the same setup as we used in I. We assume the $(p_{1/2})^2_{J=0}$ configuration for the halo neutron,

$$\phi_0(\mathbf{r}_1,\mathbf{r}_2)=[\psi_{(p_{1/2})}(\mathbf{r}_1)\psi_{(p_{1/2})}(\mathbf{r}_2)]_{J=0}\ . \tag{3.14}$$

The single particle wave function $\psi_{(p_{1/2})}(\mathbf{r})$ is constructed with the Woods-Saxon potential, whose depth is chosen so as to set the single particle binding energy equal to 0.1 MeV. As for the neutron-^{12}C optical potential, we use

the conventional Woods-Saxon potential without spin-orbit force. Parameters for the potential are the following:

$$V=37.4 \text{ MeV}, \quad r_R=1.2 \text{ fm}, \quad a_R=0.75 \text{ fm}, \\ W=10 \text{ MeV}, \quad r_I=1.3 \text{ fm}, \quad a_I=0.6 \text{ fm}. \tag{3.15}$$

The above parameters are enough for the calculation of $U_{2n}(R)$ of Eq. (3.8). To get a total ^{11}Li-^{12}C optical potential, we should add ^{9}Li-^{12}C optical potential, $U_{^9\text{Li}}(R)$, to it. At present no phenomenological potential for $U_{^9\text{Li}}(R)$ is available. We also took the Woods-Saxon potential for this case, whose parameters are chosen as

$$V=140 \text{ MeV}, \quad r_R=0.7 \text{ fm}, \quad a_R=0.9 \text{ fm}, \\ W=25 \text{ MeV}, \quad r_I=0.98 \text{ fm}, \quad a_I=0.75 \text{ fm}. \tag{3.16}$$

The radius parameter R_R is given by $r_R(9^{1/3}+12^{1/3})$.

Figure 4 shows the obtained ^{11}Li-^{12}C optical potentials. $U_{2n}(R)$ of Eq. (3.8) and the single folding result, $U_{2n}^{(1)}(R)$, of Eq. (3.11) are compared. $U_{^9\text{Li}}(R)$ is also shown for reference. The long range nature of the optical potential of the halo-neutron part is due to the spatially extended density distribution of the two neutrons which constitute the halo. As is expected, the strong effect of the break-up is seen in both the real and imaginary parts of the optical potential. The repulsive effect for the real part and the increase of the absorption are the same properties as those of the deuteron case.

Figure 5 shows the decomposition of the dynamical polarization potential into the cumulant expansion. As in the case of the deuteron shown in Fig. 3, the second-order result gives the same sign as the full dynamical polarization potential. However, the convergence of the cumulant expansion is very slow. It means that the break-up process is highly nonperturbative and the classification according to the moments of the fluctuation is not so useful, though it gives the single folding model in the lowest order.

We next investigate the energy dependence of the optical potential. Solid curves in Fig. 6 show the energy dependence of the halo-neutron contribution to the optical potential at $R=6.5$ fm. The folding model results given by Eq. (3.11) are also shown by dashed curves. The parameters for the optical potential of the n-^{12}C system is given in I. The abrupt changes of the curves at a few energies come from the different parametrization of the n-^{12}C optical potential for each energy interval. As for the real part, the dynamical polarization potential increases for low incident energy. In the low incident energy region the dynamical polarization potential is so large that it almost cancels the attractive potential due to the single folding model. The imaginary part of the optical potential due to the halo neutron is closely related to the total reaction cross section and the two-neutron removal cross

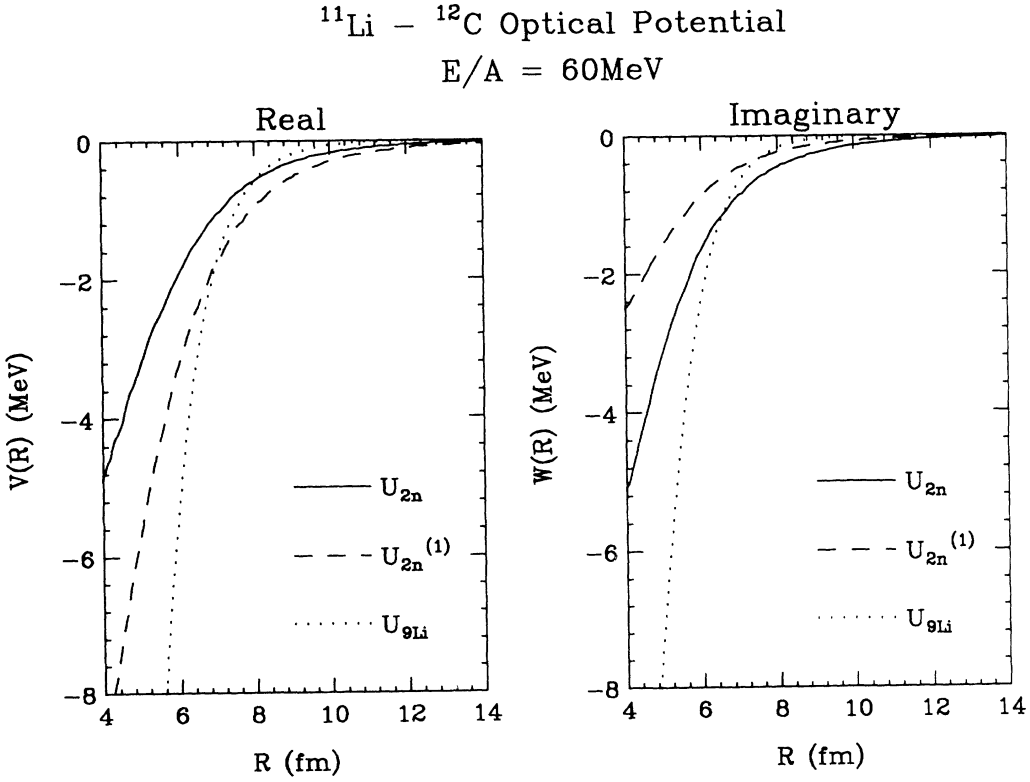

FIG. 4. The optical potential of the ^{11}Li-^{12}C system at $E=60$ MeV/nucleon. Halo-neutron contribution to the optical potential is shown by the solid curves. Halo-neutron contribution by the single folding model is also shown by dashed curves. The ^{9}Li-^{12}C optical potential assumed in our calculation is shown by dotted curves.

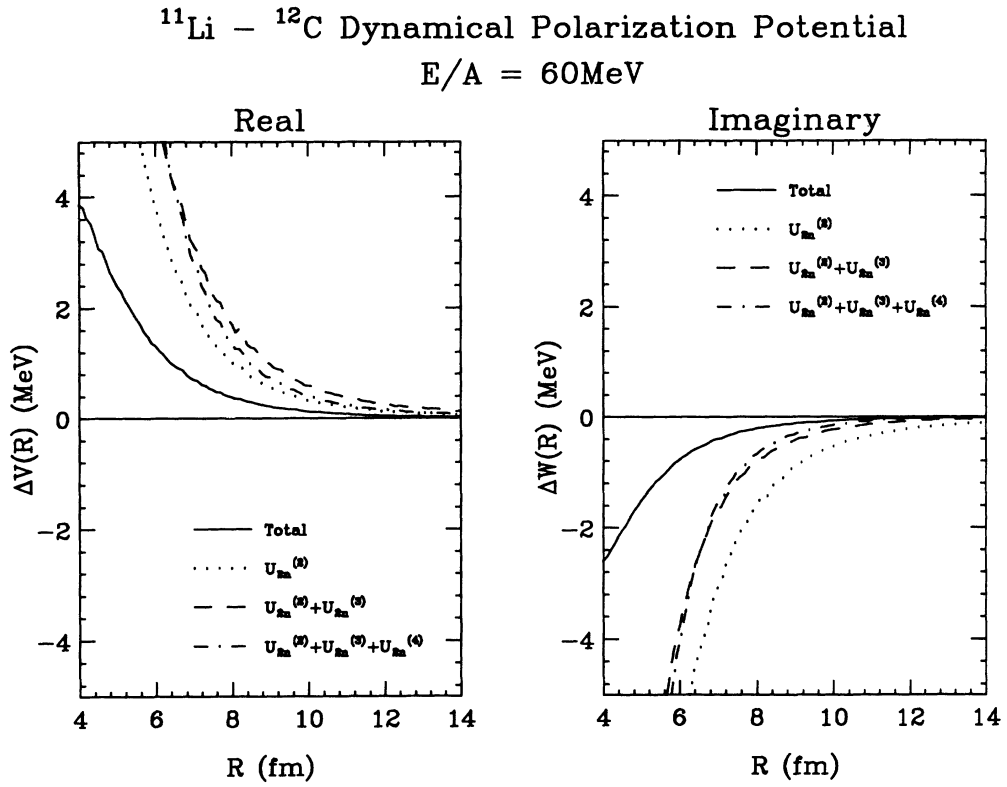

FIG. 5. The dynamical polarization potential of ^{11}Li-^{12}C and its decomposition according to the cumulant expansion.

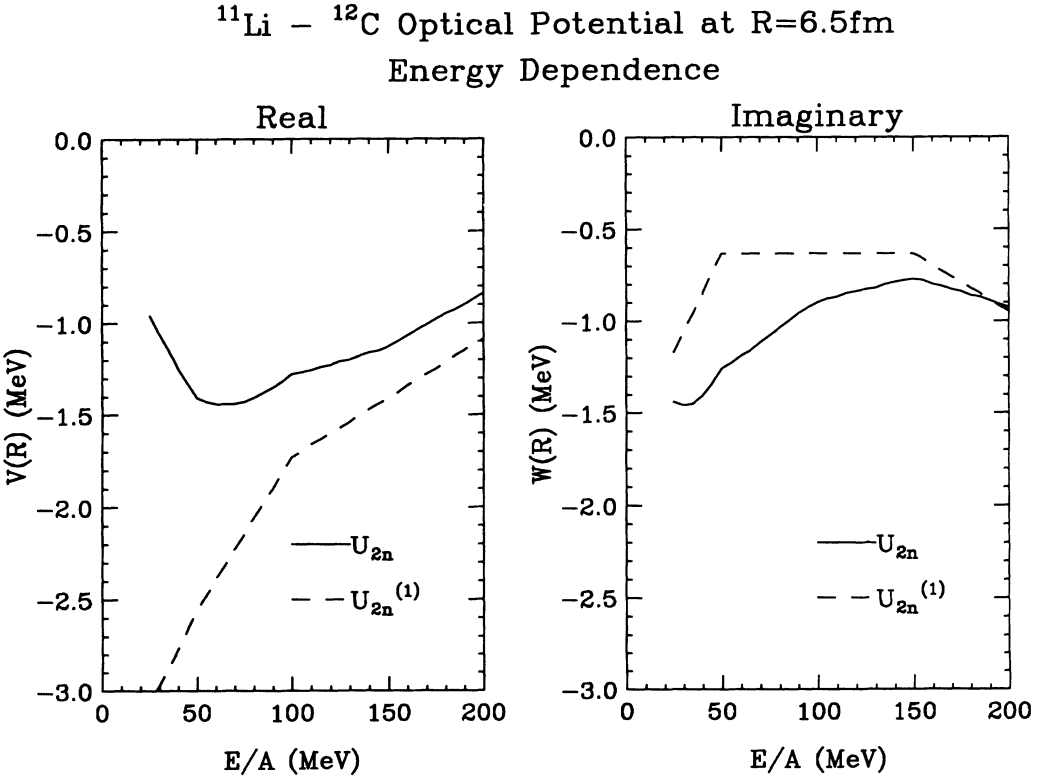

FIG. 6. The energy dependence of the halo-neutron contribution to the ^{11}Li-^{12}C optical potential at $R=6.5$ fm. Solid curves represent the halo-neutron contribution including the break-up effect. Dashed curves represent the potential by the single folding model.

section of ^{11}Li. In the energy region considered in this paper, the total reaction cross section by our theory is larger than that by the folding model as discussed in I. At the incident energy of 200 MeV/nucleon, the dynamical polarization potential almost disappears. This is consistent with the discussion given below Eq. (2.12), that is, the sign of the imaginary part of the dynamical polarization potential depends on the relative strength of the real and imaginary parts of the neutron optical potential. At about this energy, the real part of the optical potential becomes less significant than the imaginary part. Above this energy the inclusion of the break-up effect is expected to diminish the absorption. The same conclusion is obtained in the analysis of the two-neutron removal cross section at high incident energy based on the Glauber's multiple scattering theory [15].

IV. ELASTIC DIFFERENTIAL CROSS SECTION OF ^{11}Li

The differential cross section for the elastic scattering of the ^{11}Li-^{12}C system at $E/A=60$ MeV is calculated using the optical potential obtained in the preceding section and is shown in Fig. 7. The solid curve represents the result by solving quantum mechanically the Schrödinger equation with the optical potential of Eq. (3.8). The dotted curve is the differential cross section by the scattering amplitude of Eq. (3.3) under the eikonal approximation. The small difference between the solid and dotted curves indicates that the eikonal approximation in calculating the angular distribution is quite accurate for this system.

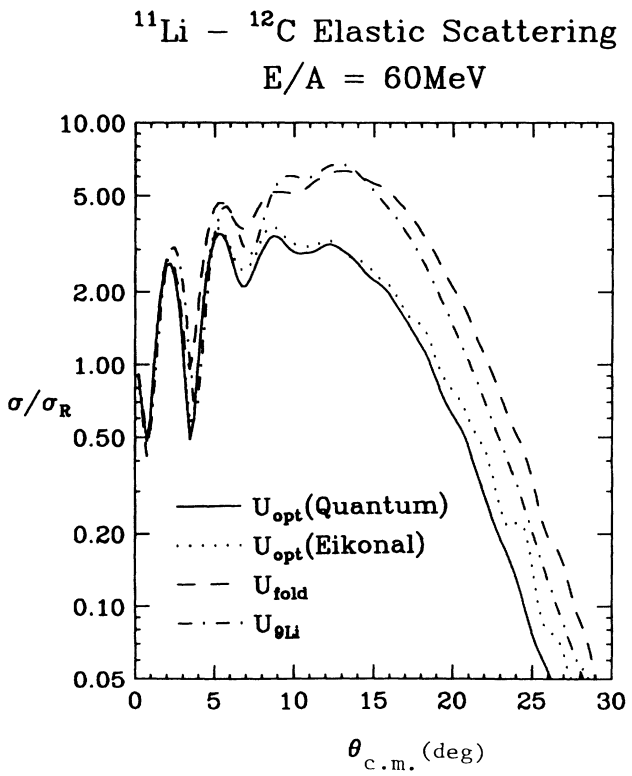

FIG. 7. The elastic scattering cross section of ^{11}Li-^{12}C at $E/A=60$ MeV. The solid curve represents the cross section with the optical potential of our theory. The dotted curve is the cross section with the same optical potential under the eikonal approximation. The dashed and dotted curves are with the potential of single folding model and the optical potential of ^{9}Li-^{12}C system, respectively.

For comparison, the cross section with the optical potential of the single folding model given by Eq. (3.11) is also shown by the dashed curve. The dot-dashed curve represents the cross section with $U_{^9\mathrm{Li}}(R)$ only, that is, the cross section when we neglect the interaction between the halo neutron and the target nucleus. In other words, it represents the cross section of ^{9}Li-^{12}C elastic scattering with the assumed optical potential of $U_{^9\mathrm{Li}}(R)$. It is however plotted in the center-of-mass frame of ^{11}Li-^{12}C.

At large scattering angles, the solid curve is much smaller than both the dashed and dot-dashed curves. Compared with the dot-dashed curve which represents ^{9}Li-^{12}C scattering, the solid and the dashed curves include the halo-neutron contribution to the optical potential. The attractive contribution to the real part of the optical potential works to increase the cross section at large angles while the absorptive contribution to decrease it. The fact that the cross section of the single folding model is close to that of ^{9}Li-^{12}C indicates that the effect of the halo contribution to the real and the imaginary parts works just to cancel each other. The inclusion of the break-up of the halo neutron contributes to weaken the real part of the optical potential and to make stronger the imaginary part. Both contributions decrease the cross section at large scattering angle. Then the solid curve predicts the small cross section of ^{11}Li-^{12}C at large scattering angle.

To investigate the role of the dynamical polarization potential in more detail, we compare the following in Fig. 8; the solid and the dashed curves are the same as those of Fig. 7, i.e., the cross section calculated with $U_{\mathrm{opt}}(R)=U_{^9\mathrm{Li}}(R)+U_{2n}(R)$ and $U_{\mathrm{fold}}(R)=U_{^9\mathrm{Li}}(R)+U_{2n}^{(1)}(R)$, respectively. The dotted curve represents the cross section where the real part of the dynamical polarization potential is included, $U_{^9\mathrm{Li}}(R)+U_{2n}^{(1)}(R)+\mathrm{Re}\Delta U(R)$. In the dot-dashed curve the imaginary part of the dynamical polarization potential is included, $U_{^9\mathrm{Li}}(R)+U_{2n}^{(1)}(R)+i\,\mathrm{Im}\Delta U(R)$. Both the real and imaginary parts of the dynamical polarization potential work to decrease the elastic differential cross section to the approximately same extent. The decrease of the cross section due to the imaginary part of the dynamical polarization potential would be simply understood by considering that the ^{11}Li nucleus is easy to break-up on receiving the large momentum transfer. The real part of the dynamical polarization potential, though it is difficult to get an intuitive picture, plays also an important role as in the case of the deuteron scattering.

The uncertainty of our calculation mainly comes from the lack of the knowledge of the ^{9}Li-^{12}C interaction. We hope that the elastic scattering cross sections of both ^{11}Li and ^{9}Li will be measured to make a definite discussion on the role of the halo neutron. At present the available data for ^{11}Li-^{12}C reaction at the intermediate energy region is only the total interaction cross section. Our analysis in I showed that it was reasonably well repro-

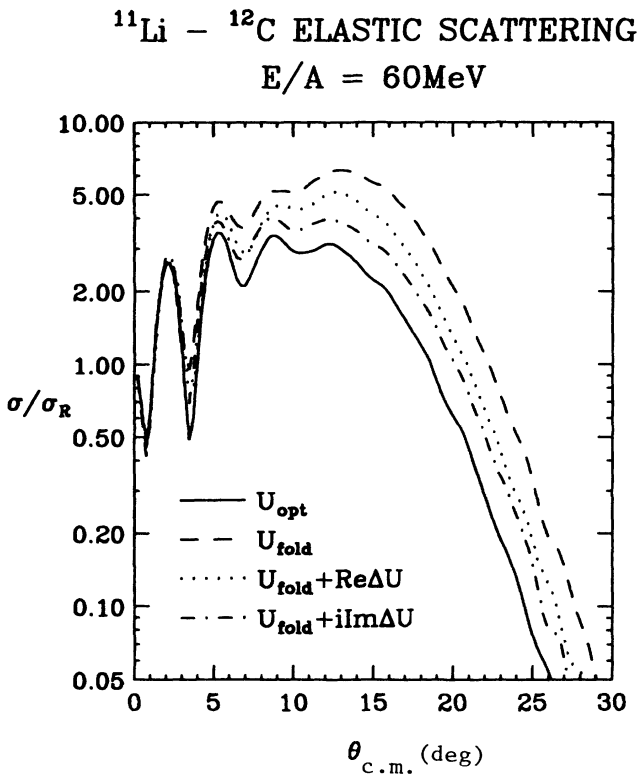

FIG. 8. The elastic scattering cross section of ^{11}Li-^{12}C at $E/A = 60$ MeV. The solid and dashed curves are the same as those of Fig. 6. The dotted and dot-dashed curves are the cross section with the inclusion of the real part and the imaginary part of the dynamical polarization potential to the single folding potential, respectively.

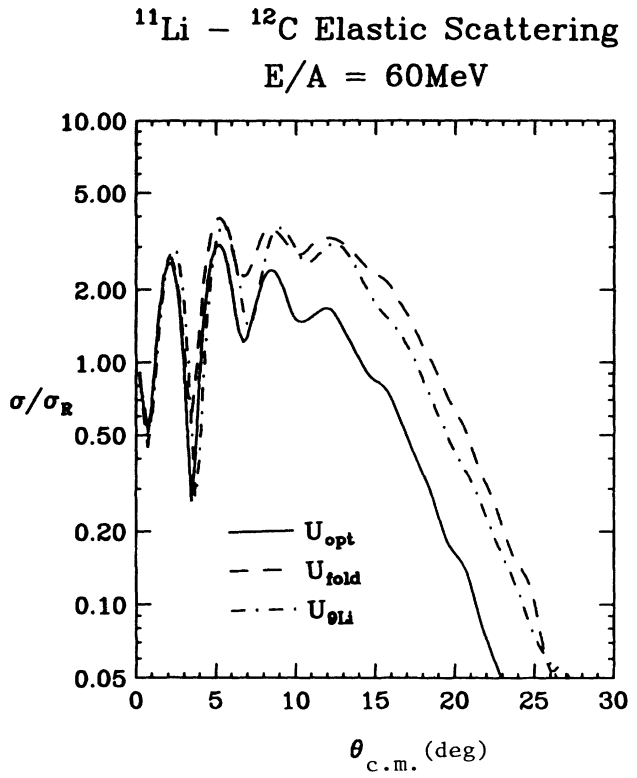

FIG. 9. The same as Fig. 7 but the parameter of the optical potential of ^{9}Li-^{12}C is slightly changed. See the text for the detail.

duced by our model. To examine the dependence of the qualitative features discussed above on the choice of the assumed ^{9}Li-^{12}C optical potential, we show in Fig. 9 the elastic differential cross section calculated when the parameter r_I in Eq. (3.16) is varied from 0.98 to 1.08 fm. It should be noted that this choice of the ^{9}Li-^{12}C optical potential would somewhat overestimate the total interaction cross section of ^{11}Li-^{12}C. The elastic scattering cross sections of Fig. 9, though small in magnitude compared with those in Fig. 7, show features qualitatively very similar to those of Fig. 7. Thus the discussion concerning the role of the halo neutron on the cross section will hold irrespective of the assumed $U_{^{9}\mathrm{Li}}(R)$ optical potential.

V. CONCLUDING REMARKS

We have discussed, on the basis of the eikonal approximation, the role of the break-up process in the optical potential and the elastic scattering of weakly bound projectiles such as deuteron and ^{11}Li nucleus.

Our framework provides us with the description of the dynamical polarization potential due to the break-up process in terms of the phase shift function. Especially the dynamical polarization potential is discussed in relation to the fluctuation of the nucleon motion of the projectile ground state. The deuteron scattering has first been treated in our theory and its results has been compared with the CDCC calculation. This test example has demonstrated that our treatment is a quite good approximation to a description of the break-up process at intermediate and high energies.

We have applied our framework to ^{11}Li-^{12}C elastic scattering at $E/A = 60$ MeV. We have found the strong effect of the break-up process both on the optical potential and on the differential cross section. As in the case of the deuteron, the break-up of the halo neutron makes a repulsive contribution to the real part and an absorptive contribution to the imaginary part of the optical potential. Because of this property, the break-up effect works to decrease the elastic scattering cross section at large scattering angle significantly compared with the folding model result. Comparison of the cross section is also made with the elastic cross section of ^{9}Li-^{12}C at the center-of-mass frame of ^{11}Li-^{12}C. Our calculation predicts that the cross section of ^{11}Li-^{12}C elastic scattering is much smaller than that of ^{9}Li-^{12}C.

ACKNOWLEDGMENTS

This work was supported in part by the Grant-in-Aid for Scientific Research (Nos. 03640265 and 03740142) of the Ministry of Education, Science and Culture. This work was also supported in part by Research Center for Nuclear Physics, Osaka University.

[1] I. Tanihata *et al.,* Phys. Rev. Lett. **55**, 2676 (1985).
[2] G. R. Satchler, K. W. McVoy, and M. S. Hussein, Nucl. Phys. **A522**, 621 (1991).
[3] L. F. Canto, R. Donangelo, and M. S. Hussein, Nucl. Phys. **A529**, 243 (1991).
[4] A. N. F. Aleixo, C. A. Bertulani, and M. S. Hussein, Phys. Rev. C **43**, 2722 (1991).
[5] Y. Tosaka and Y. Suzuki, Nucl. Phys. **A512**, 46 (1990); K. Ikeda, Proceedings of the Fifth International Conference on Nucleus-Nucleus Collision, Kanawaza, 1991 (in press).
[6] G. F. Bertsch and H. Esbensen, Ann. Phys. **209**, 327 (1991).
[7] G. R. Satchler and W. G. Love, Phys. Rep. **55**, 183 (1979).
[8] R. C. Johnson and P. J. R. Soper, Phys. Rev. C **1**, 976 (1970); H. Amakawa, A. Mori, H. Nishioka, K. Yazaki, and S. Yamaji, *ibid.* **23**, 583 (1981).
[9] M. Yahiro, Y. Iseri, H. Kameyama, M. Kamimura, and M. Kawai, Prog. Theor. Phys. Suppl. **89**, 32 (1986); Y. Iseri, M. Yahiro, and M. Kamimura, Prog. Theor. Phys. **89**, 84 (1986).
[10] Y. Sakuragi, M. Yahiro, and M. Kamimura, Prog. Theor. Phys. Suppl. **89**, 136 (1986).
[11] K. Yabana, Y. Ogawa, and Y. Suzuki, Nucl. Phys. **A539**, 295 (1992).
[12] N. Austern, Y. Iseri, H. Kameyama, M. Kamimura, M. Kawai, G. Rawitscher, and M. Yahiro, Phys. Rep. **154**, 125 (1987).
[13] R. J. Glauber, *Lectures in Theoretical Physics,* Vol. I (Interscience, New York, 1959), p. 315.
[14] E. J. Stephenson *et al.,* Phys. Rev. C **28**, 134 (1983).
[15] Y. Ogawa, K. Yabana, and Y. Suzuki, Nucl. Phys. A (in press).